Directional Control of a Miniature Tri-axial Electromagnetic Coil in a Static Magnetic Field

E.S. Hopman*, I.S.M. Khalil

University of Twente, Faculty of Engineering Technology, Drienerlolaan 5, 7522 NB, Enschede, The Netherlands
**corresponding author A.B.Author@student.utwente.nl*

ABSTRACT: In this research, a method is proposed to realise directional control of a miniaturized tri-axial electromagnetic coil using a static nonuniform unidirectional magnetic field. A mapping was composed for a relation between the desired torque and corresponding current. Using this torque-current mapping, different magnetic field configurations were evaluated. A uniform magnetic field lacks magnetic gradient, resulting in non-invertible controllability of the tri-axial coil because the controllability matrix is not full-rank. Therefore, a nonuniform magnetic field is required to enable for the inverse mapping and determination of the current based on the desired torque. To simplify implementation of the tri-axial coil in the medical world, a magnetic field generated by a Magnetic Resonance Imaging (MRI) system could be used. MRI systems can generate nonuniform unidirectional. Three different nonuniform field configurations were compared: nonuniform unidirectional fields that contained only x-gradient, nonuniform unidirectional fields that contained x- and y-gradient, and nonuniform unidirectional fields that contained x-, y- and z-gradient. The optimal field configuration was found to be a strong nonuniform unidirectional magnetic field that contained only x-gradient. However, differences in performance were relatively small and the results showed that all three field configurations show a well-conditioned mapping with current outputs that are within the desired bounds. Therefore, it is concluded that MRI systems can be used to generate strong nonuniform unidirectional magnetic fields for directional control of a miniature tri-axial electromagnetic coil.

Key words: Directional Control, Magnetic Dipole Moment, Static Magnetic Field, Tri-axial Coil Configuration

1 INTRODUCTION

Microrobots are small tetherless devices that have the potential to perform, improve and introduce new minimally invasive techniques inside the human body. The introduction of microrobots would improve healthcare by reducing recovery time, decreasing the need for sedation, and minimising discomfort experienced by patients [1]. Examples of medical applications that microrobots can perform are targeted drug delivery and therapy, biopsy sampling and endoscopic research [2, 3]. Additionally, microrobots are preferable over tethered instruments since they can reach locations inaccessible by tethered instruments *in vivo*. In the medical world, microrobots are currently used for wireless capsule endoscopy, where the movement of the capsule is mainly passive [4]. This passive movement is realised by natural bowel peristalsis. With this procedure it is possible that an incomplete visualisation of the colons occurs, after which the procedure must be repeated [5, 6]. Reliable control on the orientation of the capsule makes visualisation more efficient and eventually enlarges the applications of microrobots in the medical world.

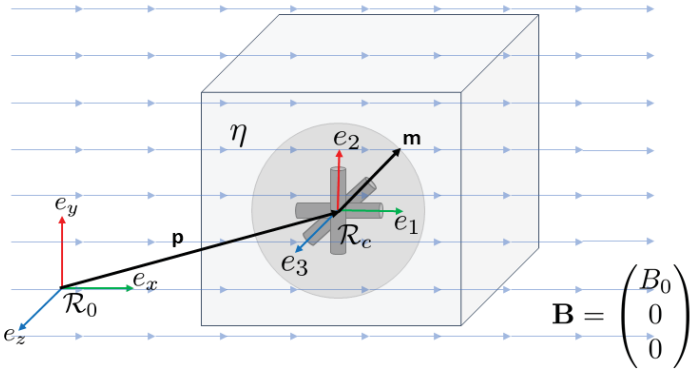

Fig. 1: Schematic overview of a miniaturised tri-axial electromagnetic coil for directional control in a medium with viscosity η. The magnetic dipole moment $\mathbf{m}$ generated by the tri-axial electromagnetic coils (defined in $\mathcal{R}_m$), tends to align with external static magnetic field $\mathbf{B}$ (defined in $\mathcal{R}_0$).

Methods for control of microrobot's motion have been widely researched in the past decade. A first method uses internal driving for translating the microrobot's body. However, the small size of microrobots puts a constraint on the power supply, limiting the generated driving force [1, 4]. A second method of re-

alising directional and translational control of microrobots makes use of external magnetic fields generated by permanent magnets or electromagnets. Magnetic force realises translation and magnetic torque realises a change in orientation of the microrobot's body [7].

There is broad spectrum of former studies done regarding wireless control of microrobots using external magnetic fields. A research performed by Kummer *et al.* [8] proposed a design of the OctoMag. This design consists of eight external coils that generate a highly nonuniform magnetic field. With this magnetic field, 5 degrees of freedom (DOF), of which 3DOF translational and 2DOF directional, control of a microrobotic agent was realised. Multiple other work, a handful of which performed by [9][10], also realised 5DOF control of a microrobot using similar electromagnetic designs as the OctoMag. Initially, 3DOF translational control was proposed [11] and realised using Helmholtz coils [12], some in combination with Maxwell coils [13, 14, 15], and saddle coils [16, 17]. All of these magnetic field generating designs consisted of at least one rotating coil pair, therefore using dynamic magnetic fields for control of the microrobot. More recent studies performed 5DOF control using Helmholtz coils [18] in combination with Maxwell coils [19], also making use of a dynamic external magnetic field.

The limiting factor on the third directional DOF of the above studies is that no driving torque can be generated around the magnetisation axis of the microrobot. Recent studies propose new designs of the microrobotic body itself that make this 6^{th} DOF possible, using external magnetic field sources similar to the OctoMag. Diller *et al.* [20] proposed a nonuniform magnetisation profile within the microrobotic body using permanent magnets, resulting in 6DOF actuation. Giltinan *et al.* [21] presented open loop control of a single-body microrobot with magnetic shape anisotropy, resulting in magnetisation components which are used to generate torque around its three axes. A last study of Petruska [22] showed that 6DOF control is possible for objects with magnetic susceptibility tensors with unique eigenvalues.

The before mentioned studies used dynamic and complex external magnetic fields generated by external coil configuration with limited workspace. Static fields can be generated by Magnetic Resonance Imaging (MRI) devices, which have larger workspace and are already present in hospitals for imaging purposes. MRI systems have the capability of generating uniform and nonuniform magnetic fields [7]. Using such magnetic fields for control of microrobots would make integration of microrobots for medical applications more appealing since no new field generating devices have to be purchased.

This paper introduces 3DOF directional control using a static magnetic field. Prior work done by Harbers *et al.* [23] proposed a method for controlling a tri-axial electromagnetic coil embedded in a microrobotic body. A schematic image of this design is shown in Fig. 1. By running electrical current through one or multiple of the tri-axial coil, a net magnetic dipole moment is generated. This magnetic dipole moment tends to align with the external magnetic field, resulting in a change of the microrobot's orientation.

The research question that will be answered in this paper is: What is the optimal static magnetic field configuration for directional control of a tri-axial electromagnetic coil? An analysis will be performed on the performance of a tri-axial electromagnetic coil in different magnetic field configurations.

2 METHODS

The proposed method for directional control of a miniature robot consists of a tri-axial electromagnetic coil system embedded in a spherical body. The miniature robot is exerted to an external static magnetic field.

2.1 Concept and Kinematics of the Miniature Robot

A schematic overview of the concept for directional control of the miniature robot is illustrated in Fig. 1. The tri-axial coil generate a controllable magnetic dipole moment $\mathbf{m} \in \mathbb{R}^{3\times1}$, described in the local material frame of reference $\mathcal{R}_m \in \mathbb{R}^{3\times1}$. $\mathcal{R}_m$ is rigidly connected to the axes of the tri-axial coil. The miniature robot is placed in a workspace that is exerted to a static magnetic field $\mathbf{B} \in \mathbb{R}^{3\times1}$, described in the fixed global frame of reference $\mathcal{R}_0 \in \mathbb{R}^{3\times1}$. The magnetic field strength is function of the miniature robot's position in the workspace. This position $\mathbf{p} \in \mathbb{R}^{3\times1}$ is defined in $\mathcal{R}_0$. Since the magnetic moment tends to align with the external magnetic field, the miniature robot will experience a torque $\boldsymbol{\tau}_m \in \mathbb{R}^{3\times1}$ as illustrated in Fig. 2. The miniature robot is located in a fluid with viscosity η, to replicate a small Reynolds

number. Reynolds number is defined as:

$$Re = \frac{\rho v L}{\eta} \tag{1}$$

where ρ is the fluid density, v is the velocity of the flow and L is the characteristic length. Equation 1 shows the ratio of the inertia terms to the viscous terms of a fluid. As microrobots are millimeter to micrometer sized objects, the inertia term in Re is very small. Due to this small size of microrobots, Reynolds number is typically < 10 [24]. Consequently, inertia terms become negligible in the fluid.

The angles that represent a difference in orientation of $\mathcal{R}_m$ and $\mathcal{R}_0$ are defined as:

$$\mathbf{\Theta} = \begin{pmatrix} \phi \\ \theta \\ \psi \end{pmatrix} \tag{2}$$

where ϕ, θ and ψ correspond to rotation of the tri-axial coil around the e_1-, e_2- and e_3-axis, respectively. In order to represent $\mathcal{R}_m$ in $\mathcal{R}_0$, the following rotation matrices are defined:

$$\mathbf{R_x} = \begin{pmatrix} 1 & 0 & 0 \\ 0 & \cos\phi & -\sin\phi \\ 0 & \sin\phi & \cos\phi \end{pmatrix}$$

$$\mathbf{R_y} = \begin{pmatrix} \cos\theta & 0 & \sin\theta \\ 0 & 1 & 0 \\ -\sin\theta & 0 & \cos\theta \end{pmatrix} \tag{3}$$

$$\mathbf{R_z} = \begin{pmatrix} \cos\psi & -\sin\psi & 0 \\ \sin\psi & \cos\psi & 0 \\ 0 & 0 & 1 \end{pmatrix}.$$

The order of the rotational matrix multiplications is based on 3-2-1 Euler intrinsic angels, and is given by:

$$\begin{pmatrix} e_1 \\ e_2 \\ e_3 \end{pmatrix} = \mathbf{R_z}(\psi)\mathbf{R_y}(\theta)\mathbf{R_x}(\phi) \begin{pmatrix} e_x \\ e_y \\ e_z \end{pmatrix}. \tag{4}$$

This order is used since better control on the roll motion of the miniature robot can be realised, which is favorable for additional propulsion generation [23].

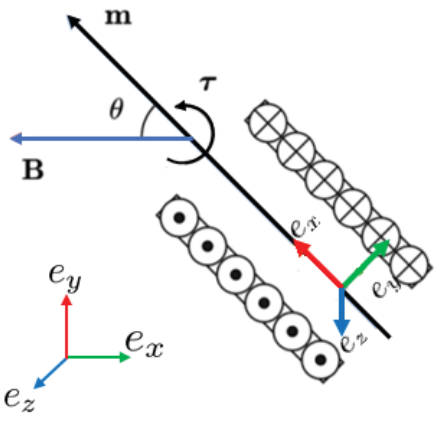

Fig. 2: Schematic overview magnetic dipole moment $\mathbf{m}$ generated by one coil. If an angle $\boldsymbol{\theta}$ is present between the direction of $\mathbf{m}$ and $\mathbf{B}$, a torque is generated. This torque aligns the magnetic moment with the external magnetic field. [23]

2.2 *Magnetic Actuation*

Magnetic actuation of the tri-axial coils is initiated by generating a magnetic dipole moment. The magnetic dipole moment generated by the tri-axial electromagnetic coils is defined by:

$$\mathbf{m} = NS\mathbf{I} \tag{5}$$

where N is the number of turns, S is the area enclosed by one coil loop and $\mathbf{I} \in \mathbb{R}^{3\times1}$ is the current running through the coils. The magnetic torque due to the magnetic moment and the magnetic field is defined as:

$$\boldsymbol{\tau_m} = \mathbf{m} \times \mathbf{B}. \tag{6}$$

In case of a nonuniform magnetic field, the miniature robot experiences a magnetic force. The force exerted on the miniature robot is described as:

$$\mathbf{f_m} = \nabla(\mathbf{B} \cdot \mathbf{m}). \tag{7}$$

The drag force and torque of a spherical body in low Reynolds number are described by Stokes' law [24]:

$$\begin{aligned} \mathbf{f}_d &= 6\pi r\eta\mathbf{V} \\ \boldsymbol{\tau}_d &= 8\pi r^3\eta\boldsymbol{\Omega} \end{aligned} \tag{8}$$

where r is the radius of the spherical body which contains the tri-axial coil, $\mathbf{V} \in \mathbb{R}^{3\times1}$ and $\boldsymbol{\Omega} \in \mathbb{R}^{3\times1}$ are the linear and angular velocity, respectively. As

discussed in Section 2.1 low Reynolds number is assumed and therefore the inertia terms are negligible in the equations of motion, which are defined by:

$$\begin{aligned} \mathbf{f}_d + \mathbf{f}_m &= 0 \\ \boldsymbol{\tau}_d + \boldsymbol{\tau}_m &= 0 \end{aligned} \tag{9}$$

where the only components acting on the miniature robot are the magnetic and drag force and torque.

2.3 Torque-current Mapping

For directional control, a function is required that maps the desired torque with the corresponding current for the tri-axial coil. Equation 6 is rewritten in skew-symmetric matrix form such that:

$$\begin{aligned} \boldsymbol{\tau}_m &= \mathbf{m} \times \mathbf{B} \\ &= -\mathbf{B} \times \mathbf{m} \\ &= -\mathrm{Sk}(\mathbf{B})\mathbf{m}. \end{aligned} \tag{10}$$

$\mathrm{Sk}(\mathbf{B})$ represents the skew-symmetric matrix of $\mathbf{B}$ and is described as:

$$-\mathrm{Sk}(\mathbf{B}) = \begin{pmatrix} 0 & B_z & -B_y \\ -B_z & 0 & B_x \\ B_y & -B_x & 0 \end{pmatrix}. \tag{11}$$

Writing $\mathbf{m}$ as function of $\boldsymbol{\tau}_m$ would require the inverse of $\mathrm{Sk}(\mathbf{B})$. This is not possible, since the inverse of a skew-symmetric matrix would go to infinity. In addition, the tri-axial coil requires control in three directions. Since the rank of $\mathrm{Sk}(\mathbf{B})$ equals 2, a mapping based on only the magnetic torque equation results in an incomplete control system. Therefore, the magnetic force, defined in Equation 7, is considered as well. The magnetic force is described as:

$$\begin{aligned} \mathbf{f} &= \nabla(\mathbf{B} \cdot \mathbf{m}) \\ &= \left(\tfrac{\partial B_x}{\partial x} + \tfrac{\partial B_y}{\partial y} + \tfrac{\partial B_z}{\partial z}\right) \begin{pmatrix} m_x \\ m_y \\ m_z \end{pmatrix} \\ &= \begin{pmatrix} \frac{\partial B_x}{\partial x} m_x + \frac{\partial B_y}{\partial y} m_x + \frac{\partial B_z}{\partial z} m_x \\ \frac{\partial B_x}{\partial x} m_y + \frac{\partial B_y}{\partial y} m_y + \frac{\partial B_z}{\partial z} m_y \\ \frac{\partial B_x}{\partial x} m_z + \frac{\partial B_y}{\partial y} m_z + \frac{\partial B_z}{\partial z} m_z \end{pmatrix}. \end{aligned} \tag{12}$$

Merging Equation 10 and 12 gives the combined magnetic force-torque vector:

$$\left(\begin{array}{c} f_x \\ f_y \\ f_z \\ \hline \tau_x \\ \tau_y \\ \tau_z \end{array}\right) = \left(\begin{array}{ccc} \frac{\partial}{\partial x} B_x & \frac{\partial}{\partial y} B_x & \frac{\partial}{\partial z} B_x \\ \frac{\partial}{\partial x} B_y & \frac{\partial}{\partial y} B_y & \frac{\partial}{\partial z} B_y \\ \frac{\partial}{\partial x} B_z & \frac{\partial}{\partial y} B_z & \frac{\partial}{\partial z} B_z \\ \hline 0 & B_z & -B_y \\ -B_z & 0 & B_x \\ B_y & -B_x & 0 \end{array}\right) \begin{pmatrix} m_x \\ m_y \\ m_z \end{pmatrix} \tag{13}$$

$$\boldsymbol{\Gamma} = \mathbf{A}(\mathbf{p})\mathbf{m}$$

where $\boldsymbol{\Gamma} \in \mathbb{R}^{6\times 1}$ is the force-torque vector, $\mathbf{A}(\mathbf{p}) \in \mathbb{R}^{6\times 3}$ is the mapping matrix, and $\mathbf{m}$ is the magnetic moment of the tri-axial coil. As magnetic field $\mathbf{B}$ is function $\mathbf{p}$, and the mapping matrix consists solely out of components of $\mathbf{B}$, mapping matrix $\mathbf{A}$ is also considered to be function of $\mathbf{p}$.
Since $\mathbf{A}(\mathbf{p})$ is an asymmetric matrix, its pseudo-inverse, defined by $\mathbf{A}^\dagger(\mathbf{p}) \in \mathbb{R}^{3\times 6}$, is used to write $\mathbf{m}$ as function of $\boldsymbol{\Gamma}$:

$$\begin{aligned} \mathbf{m} &= \mathbf{A}^\dagger(\mathbf{p})\boldsymbol{\Gamma} \\ NS\mathbf{I} &= \mathbf{A}^\dagger(\mathbf{p})\boldsymbol{\Gamma}. \end{aligned} \tag{14}$$

The pseudo-inverse is formed by the singular value decomposition of $\mathbf{A}(\mathbf{p})$. This singular value decomposition is defined as $\mathbf{A} = \mathbf{USV}^T$. $\mathbf{U}$ and $\mathbf{V}$ are orthogonal real or complex matrices, and $\mathbf{S}$ is a rectangular diagonal matrix that consists of the singular values of $\mathbf{A}$ on the diagonal [8]. The singular values and can be used to verify the condition of the mapping matrix. A measure for the condition of a matrix is called the condition number. The condition number shows the sensitivity of the output to a small change of the input. If this sensitivity is low, the condition number is also low, resulting in a good conditioned matrix [25]. The condition number is a function of the highest and lowest singular value, σ_{max} and σ_{min} respectively. The condition number CN is defined as [26]:

$$\mathrm{CN} = \frac{\sigma_{max}}{\sigma_{min}} \tag{15}$$

A well-conditioned matrix has a condition number close to 1. The singular values are defined by components of mapping $\mathbf{A}$. Since $\mathbf{A}$ consists of magnetic field parameters that are function of position $\mathbf{p}$, the condition number depends the position.

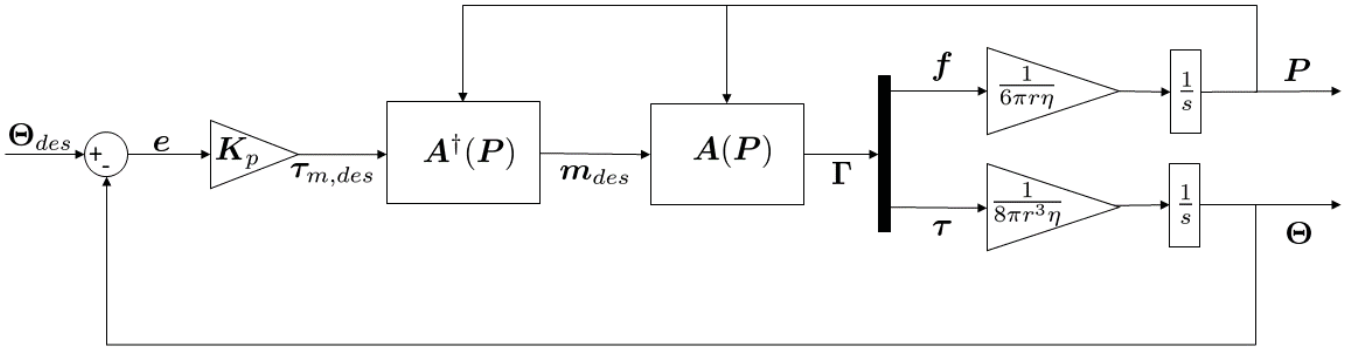

Fig. 3: Block diagram of the tri-axial coil system implemented with full state feedback control.

2.4 Full State Feedback Control

For directional control of the microrobot, a full state feedback controller will be used. Full state feedback is based on state-space equations:

$$\begin{aligned} \dot{\mathbf{x}} &= \mathbf{A}\mathbf{x} + \mathbf{B}\mathbf{u} \\ \mathbf{y} &= \mathbf{C}\mathbf{x} + \mathbf{D}\mathbf{u} \end{aligned} \tag{16}$$

where $\mathbf{u}$ is the input of the system, $\mathbf{y}$ is the output of the system, $\mathbf{x}$ is the state vector, $\mathbf{A}$ is the system matrix, $\mathbf{B}$ is the input matrix, $\mathbf{C}$ is the output matrix, and $\mathbf{D}$ is the feed-through matrix. If the input $\mathbf{u}$ is chosen to be a constant $\mathbf{K}$ multiplied with state $\mathbf{x}$, such that $\mathbf{u} = -\mathbf{K}\mathbf{x}$, Equation 16 can be written as:

$$\begin{aligned} \dot{\mathbf{x}} &= \mathbf{A}\mathbf{x} - \mathbf{B}\mathbf{K}\mathbf{x} \\ &= (\mathbf{A} - \mathbf{B}\mathbf{K})\mathbf{x}. \end{aligned} \tag{17}$$

When a system is full rank, stability is realised if the requirement $(\mathbf{A} - \mathbf{B}\mathbf{K}) \leq \mathbf{0}$ is met.

For the tri-axial coils, a desired orientation $\boldsymbol{\Theta}_{des} \in \mathbb{R}^{3\times1}$ is defined as the system input. An error $\mathbf{e} \in \mathbb{R}^{3\times1}$ is defined by the difference between $\boldsymbol{\Theta}$ and $\boldsymbol{\Theta}_{des}$. Taking the time derivative of this error gives the angular velocity:

$$\begin{aligned} \boldsymbol{e} &= \boldsymbol{\Theta}_{des} - \boldsymbol{\Theta} \\ \dot{\boldsymbol{e}} &= \dot{\boldsymbol{\Theta}} = \boldsymbol{\Omega} \end{aligned} \tag{18}$$

When the desired magnetic torque is set to $\boldsymbol{\tau}_{m,des} = \mathbf{K}_p\mathbf{e}$, where $\mathbf{K}_p \in \mathbb{R}^{3\times1}$ is a controller gain, the torque equation of motion from Equation 9 can be written as a differential equation:

$$\begin{aligned} \boldsymbol{\tau}_{m,des} + \boldsymbol{\tau}_d &= 0 \\ \mathbf{K}_p\mathbf{e} + 8\pi r^3\eta\dot{\mathbf{e}} &= 0. \end{aligned} \tag{19}$$

This differential equation allows full state feedback control to be applied. Rewriting Equation 19 gives:

$$\dot{\boldsymbol{e}} = -\frac{\mathbf{K}_p}{8\pi r^3\eta}\boldsymbol{e}. \tag{20}$$

This equation is written in a similar way as Equation 17. A controller $\mathbf{K}_p$ has to be designed such that the term before $\mathbf{e}$ in Equation 20 is smaller or equal to zero ($-\frac{K_p}{8\pi r^3\eta} \leq 0$), which realises a stable system.
The above described method of control can also be applied to the force equation of motion. A block diagram of the system with full state feedback control is shown in Fig. 3.

2.5 Magnetic Field Configuration

A uniform magnetic field configuration has constant magnitude and direction. A uniform magnetic field can consist of an x-, y- and z-component, as long as there is no magnetic gradient present. Due to a lack in magnetic gradients, mapping $\mathbf{A}$ for uniform magnetic fields consists of only zeros in its first three rows. The skew-symmetric part remains in the fourth to sixth row, similar to Equation 10. Therefore the rank of $\mathbf{A}$ for a uniform magnetic field equals 2, which is not full rank. The condition number of $\mathbf{A}$ for a uniform field would go to infinity for every position in the workspace, resulting in an ill-conditioned matrix.
Nonuniform magnetic fields contain magnetic gradients. Similar to uniform magnetic fields, nonuniform magnetic fields can have an x-, y- and z-component. Mapping $\mathbf{A}$ for nonuniform magnetic fields contain at least one nonzero element in the first three rows. Therefore, the mapping for nonuniform magnetic fields is full rank, making it possible to control the three directions of the tri-axial coils independently.

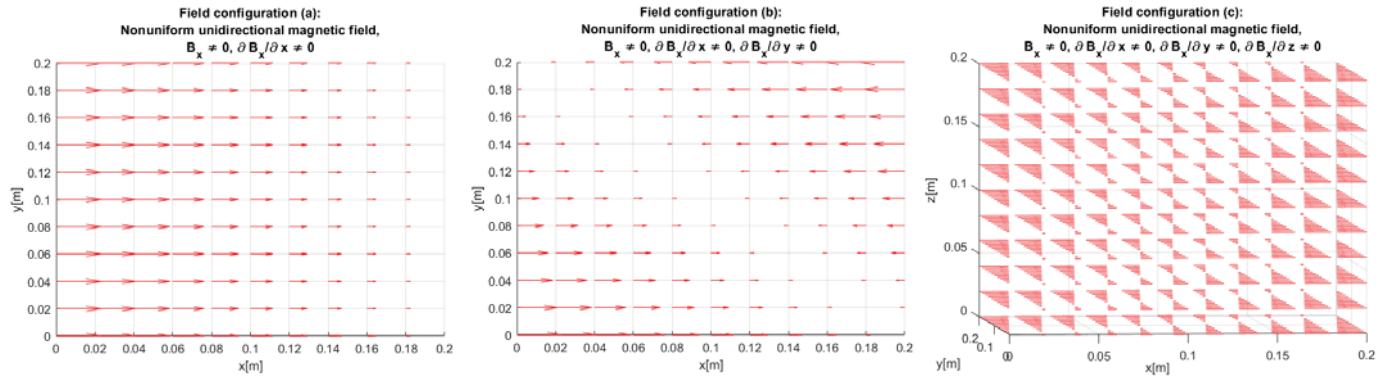

(a) Magnetic field configuration (a), where $B_x \neq 0$ and $\frac{\partial B_x}{\partial x} \neq 0$

(b) Magnetic field configuration (b), where $B_x \neq 0$, $\frac{\partial B_x}{\partial x} \neq 0$ and $\frac{\partial B_x}{\partial y} \neq 0$

(c) Magnetic field configuration (b), where $B_x \neq 0$, $\frac{\partial B_x}{\partial x} \neq 0$, $\frac{\partial B_x}{\partial y} \neq 0$ and $\frac{\partial B_x}{\partial z} \neq 0$

Fig. 4: Three nonuniform unidirectional field configurations that can be generated by MRI systems.

MRI systems are able to generate nonuniform unidirectional magnetic fields, with gradients in x-, y- and z-direction. This research wants to find out if MRI systems are usable for directional control of tri-axial electromagnetic coils. Therefore, three nonuniform unidirectional magnetic field configurations will be evaluated: only x-gradient (a), x- and y-gradient (b), and x- y- and z-gradient (c). The nonuniform unidirectional magnetic field configurations are illustrated in Fig. 4.

Nonuniform multidirectional magnetic field have been shortly reviewed as well. However, these field types cannot be generated by MRI systems and they did not show significantly better condition number than unidirectional fields. Therefore, multidirectional magnetic fields are not evaluated in this research

3 RESULTS

3.1 Condition Number as Function of Position

The condition number depends on the position $\mathbf{p}$ defined in the global frame of reference. The condition number is plotted over a workspace of 1.5 by 1.5 m for magnetic field configuration (a), (b) and (c), which is illustrated in Fig. 6. For this plots, it is assumed that the magnetic gradients are constant and identical for x-, y- and z-direction, with a value of 0.04 T/m for. The condition numbers are plotted in x, y-plane.

Fig. 6 show where in the workspace the condition number is low. The lowest condition number for magnetic field configuration (a), (b) and (c) are respectively: CN_a = 1.414, CN_b = 1.622 and CN_c = 1.624. The position where the condition number is lowest is further evaluated. The positions with lowest condition number for magnetic field configuration (a), (b) and (c) are respectively: $\mathbf{p}_a$ = [1.5 0 0]m, $\mathbf{p}_b$ = [0 1.1 0]m and $\mathbf{p}_a$ = [0 0.8 0]m.

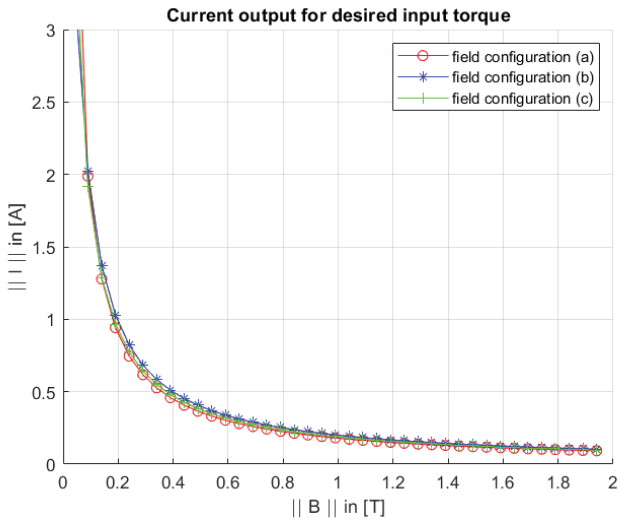

Fig. 5: Desired current as function of the magnetic field strength, given a desired input $\mathbf{\Gamma}$

3.2 Magnetic Field Strength

To confirm whether the condition numbers defined in Section 3.1 are in agreement with the numerical outcome of Equation 14, Fig. 5 illustrates the relation of the current to the strength of the nonuniform magnetic field. The differences is the three field configurations is very small. It is barely notable in the figure, but from $\| B \| > 0.2$T the desired current for field configuration (a) lowest compared to the other configurations.

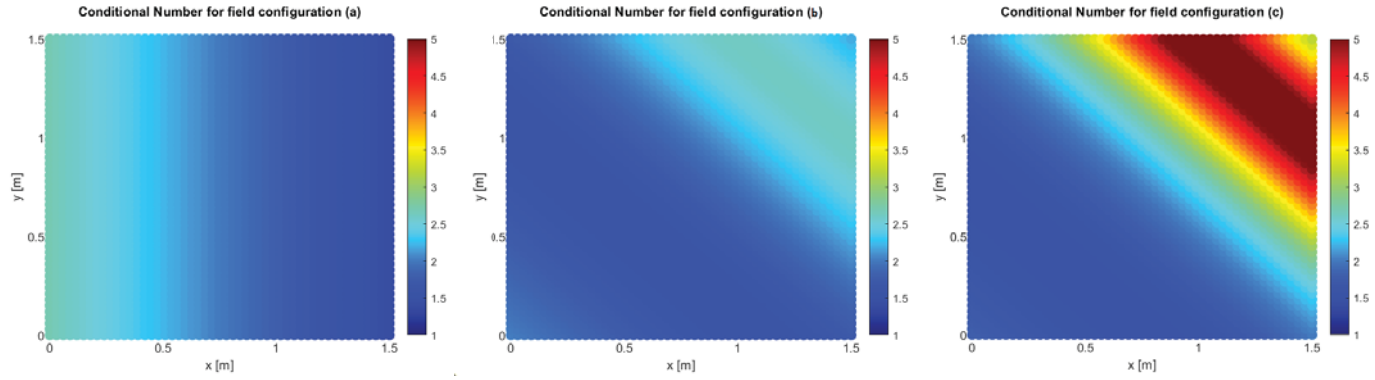

(a) CN of field configuration (a), lowest value of CN_a = 1.414 at $\mathbf{p}_a$ = [1.5 0 0]m **(b)** CN of field configuration (b), lowest value of CN_b = 1.622 at $\mathbf{p}_b$ = [0 1.1 0]m **(c)** CN of field configuration (c), lowest value of CN_c = 1.583 at $\mathbf{p}_a$ = [0 0.8 0]m

Fig. 6: Condition Number (CN) of the three nonuniform unidirectional field configurations plotted over workspace of 1.5m by 1.5m.

4 DISCUSSION

Uniform magnetic fields cannot be used for 3DOF directional control of the tri-axial electromagnetic coil, because the torque-current mapping does not show not full rank. In result, the condition number for a uniform magnetic field goes to infinity, resulting in a bad conditioned mapping.

Fig. 6 shows the condition numbers for three nonuniform magnetic field configurations. The positions were defined where the condition numbers were lowest. These positions show where the torque-current mapping is best conditioned for receiving a desired current that is best within bounds.

To validate whether the best conditioned mapping translates to the best current output for a desired torque, the relation between for the current and the magnetic field strength was illustrated in Fig. 5. The field configurations show much similarities and are almost identical graphs. All field configurations show a decreasing desired current for increasing magnetic field strength. The lowest condition number was found for field configuration (a). Field configuration (a) also showed the lowest current required for $\| B \| > 0.2$T. If the input current is low, this could simplify the design of the tri-axial coil. With low current input, less heat will be generated in the tri-axial coil. Less heat might elongate the operation time of the system. Therefore the maximum current is set to $\| I \| < 0.02$A which is met for $\| B \| > 1.0$T. Since the three field configurations are very similar, they could all be used for the directional control of the tri-axial electromagnetic coil. Besides the small differences, field configuration (a) shows the best conditioned matrix and relatively the lowest desired current. To conclude, an optimal field configuration for the system could be a strong, nonuniform, unidirectional magnetic field containing of only x-gradient. This field type can be generated by MRI systems. MRI can be used for directional control, this simplifies implementing application in the medical world, since MRI systems are already existing field generating sources in every hospital.

To validate the results obtained in this research a prototype was designed, as proposed in Appendix A. Powering of the coils was done through the copper wires of the coils. These copper wires were connected to control boards for power supply. However, it was not taken into account that the stiffness of these copper wires was relatively high. The stiffness possibly prevented the tri-axial coil from rotating when exerted to an external magnetic field. Future prototypes should account for stiffness of wires or propose for example tetherless power supplies.

5 CONCLUSIONS

Directional control of a tri-axial electromagnetic coil using a static magnetic field was investigated in this research. The magnetic field configuration the tri-axial coil would be exerted to was evaluated. Uniform magnetic fields showed a system that was not full rank. Therefore, a nonuniform magnetic field configuration was required. Three nonuniform unidirectional magnetic field configurations were compared for condition number and desired current input given a desired torque. The results showed very lit-

tle differences for the three field configurations. The best field configuration, which had the best conditioned torque-current mapping and showed the lowest desired current input, is a strong nonuniform unidirectional magnetic field that consists only of x-gradient. This field configuration can be generated by MRI systems.
To realise directional control, the tri-axial electromagnetic coil has to be exerted to a nonuniform magnetic field. As this magnetic field configuration shows a full rank torque-current mapping, full state feedback control can be applied.
Due to the lowest condition number and the lowest desired current, the optimal nonuniform magnetic field configuration showed to be a strong .

6 FUTURE WORK

Future work includes the design of a prototype where the influence of the stiffness of the copper wires on the prototype is limited or negligible. A way of doing this is to design tetherless actuation of the tri-axial electromagnetic coils. This improved prototype design could then be tested in a strong nonuniform unidirectional nonuniform magnetic field with x-gradients, as discussed in Section 4, for directional control.
A next step could be adding a translation method to the design. One method for translation that could be investigated is propulsion through a helical tail. The addition of translational control would introduce 6DOF control of the microrobot.

REFERENCES

[1] Gastone Ciuti et al. “Frontiers of robotic endoscopic capsules: a review”. In: *Journal of Micro-Bio Robotics* 11 (June 2016), pp. 1–18.

[2] Gastone Ciuti, Arianna Menciassi, and Paolo Dario. “Capsule endoscopy: From current achievements to open challenges”. In: *IEEE Reviews in Biomedical Engineering* 4 (2011), pp. 59–72.

[3] Bradley J. Nelson, Ioannis K. Kaliakatsos, and Jake J. Abbott. “Microrobots for Minimally Invasive Medicine”. In: *Annual Review of Biomedical Engineering* 12.1 (July 2010), pp. 55–85.

[4] P. Dario A. Menciassi M.Quirini. “Microrobotics for future gastrointestinal endoscopy”. In: *Minimally Invasive Therapy & Allied Technologies* (2007), pp. 91–100.

[5] Anastasios Koulaouzidis et al. “Wireless endoscopy in 2020: Will it still be a capsule?” In: *World Journal of Gastroenterology* 21.17 (2015), pp. 5119–5130.

[6] Mahesh K. Goenka, Shounak Majumder, and Usha Goenka. “Capsule endoscopy: Present status and future expectation”. In: *World Journal of Gastroenterology* 20.29 (Aug. 2014), pp. 10024–10037.

[7] Tiantian Xu et al. “Magnetic actuation based motion control for microrobots: An overview”. In: *Micromachines* 6.9 (2015), pp. 1346–1364.

[8] Michael P. Kummer et al. “Octomag: An electromagnetic system for 5-DOF wireless micromanipulation”. In: *IEEE Transactions on Robotics* 26.6 (Dec. 2010), pp. 1006–1017.

[9] M S Sakar et al. “Non-Contact, 3D Magnetic Biomanipulation for In Vivo and In Vitro Applications”. In: *Symposium on Optomechatronic Technologies* (2012), pp. 37–38.

[10] Franziska Ullrich et al. “Automated capsulorhexis based on a hybrid magnetic-mechanical actuation system”. In: *Proceedings - IEEE International Conference on Robotics and Automation* (2014), pp. 4387–4392.

[11] S. Nakamura et al. “Electromagnetic drive of microrobot geometrically constrained in blood vessel”. In: *Proceedings of the Annual International Conference of the IEEE Engineering in Medicine and Biology Society, EMBS* 1 (2011), pp. 6664–6667.

[12] Tiantian Xu et al. “Planar Path Following of 3-D Steering Scaled-Up Helical Microswimmers.” In: *IEEE Transactions on Robotics, Institute of Electrical and Electronics Engineres (IEEEE)* 31.1 (2015), pp. 117–127.

[13] Semi Jeong et al. “Novel electromagnetic actuation (EMA) method for 3-dimensional locomotion of intravascular microrobot”. In: *Sensors and Actuators, A: Physical* 157.1 (2010), pp. 118–125.

[14] Semi Jeong et al. “Remote controlled microrobots using electromagnetic actuation (EMA) systems”. In: *Proceedings of the IEEE RAS and EMBS International Conference on Biomedical Robotics and Biomechatronics* (2012), pp. 482–487.

[15] Hyunchul Choi et al. “3-D Locomotive and Drilling Microrobot Using Novel Stationary EMA Systems”. In: *IEEE/ASME Transactions on Mechatronics* 18.3 (2013), pp. 1221–1225.

[16] Hyunchul Choi et al. “EMA system with gradient and uniform saddle coils for 3D locomotion of microrobot”. In: *Sensors and Actuators, A: Physical* 163.1 (2010), pp. 410–417.

[17] Jaekwang Nam et al. “Magnetic navigation system utilizing resonant effect to enhance magnetic field applied to magnetic robots”. In: *IEEE Transactions on Industrial Electronics* 64.6 (2017), pp. 4701–4709.

[18] Mohammad Salehizadeh and Eric Diller. “Three-dimensional independent control of multiple magnetic microrobots via inter-agent forces”. In: *International Journal of Robotics Research* (2020), pp. 1–20.

[19] Kim Tien Nguyen et al. “Medical Microrobot — A Drug Delivery Capsule Endoscope with Active Locomotion and Drug Release Mechanism: Proof of Concept”. In: *International Journal of Control, Automation and Systems* 18.1 (2020), pp. 65–75.

[20] Eric Diller et al. “Six-degree-of-freedom magnetic actuation for wireless microrobotics”. In: *The International Journal of Robotics Research* 35.1-3 (Jan. 2016), pp. 114–128.

[21] Joshua Giltinan and Metin Sitti. “Simultaneous six-degree-of-freedom control of a single-body magnetic microrobot”. In: *IEEE Robotics and Automation Letters* 4.2 (2019), pp. 508–514.

[22] Andrew J. Petruska. “Open-loop orientation control using dynamic magnetic fields”. In: *IEEE Robotics and Automation Letters* 5.4 (2020), pp. 5472–5476.

[23] Abraham G. J. Harbers and Islam S.M. Khalil. “Control of a Tetherless Miniature Robot using Static Magnetic Fields”. In: *ME Bachelor Assignments proceedings 1 & 2 july* (2020), pp. 25–34.

[24] J.J. Abbott et al. “Robotics in the Small, Part I: Microbotics”. In: *IEEE Robotics & Automation Magazine* 14.2 (2007), pp. 92–103.

[25] David A. Belsley, Edwin Kuh, and Roy E. Welsch. *Regression Diagnostics: Identifying Influential Data and Sources of Collinearity*. 2005, pp. 100–103.

[26] Jianhong Shen. “On the singular values of Gaussian random matrices”. In: *Linear Algebra and Its Applications* 326.1-3 (Mar. 2001), pp. 1–14.

A PROTOTYPE DESIGN

The initial goal of the research was to show directional control of a tri-axial electromagnetic coil by designing a miniaturised prototype. The prototype consists of three orthogonal coils corresponding to the miniature robot's e_1-, e_2-, and e_3-axis. The three orthogonal coils are identical in design. The miniature robot would be tested in a fluid, therefore a spherical body was designed to surround the tri-axial coils. This spherical body consisting of the tri-axial coil is shown in Fig. 7.

Fig. 7: Design of the tri-axial electromagnetic coils embedded in a silicon spherical body. The coils are winded around a 3D-printed Polybuthylene Succinate (PBS) base (in white).

The base of the tri-axial coil configuration was 3D printed with Polybutylene Succinate (PBS) and consists of a hollow cylinder. This hollow cylinder could be filled with a ferromagnetic rod for increasing the magnetic moment if this was desired.
The coils are made from enamelled copper wire, with a diameter of 0.25mm. The number of turns is 124 and the inner diameter of the coils is 4.0mm.
The function *fmincon* in MATLAB's optimization toolbox was used to solve Equation 6 for a maximisation of the magnetic torque given a restricted number of coil turns that would fit on the base.
The tri-axial coil configuration was placed inside a 3D printed PBS mold. This mold contains a spherical cavity with a diameter of 25mm, which was filled with silicon to make the miniature robot's spherical body.

Equation 6 was used to calculate the theoretical magnetic torque that was generated by the interaction between the magnetic moment and the external magnetic field. The theoretical magnetic torque was 12 mNm. The values used for this calculation can be found in Table 1.

Before experiments were done in a fluid with high viscosity to resemble low Reynolds number, tests were done with the prototype hanging in air. The copper wires of the coils connected the prototype to a control board and power supply. The tri-axial coil was hung on these copper wires. A nonuniform magnetic field source was located next to the prototype. The magnetic field source was a permanent magnet called the SEMA. The setup can be seen in Fig. 8.

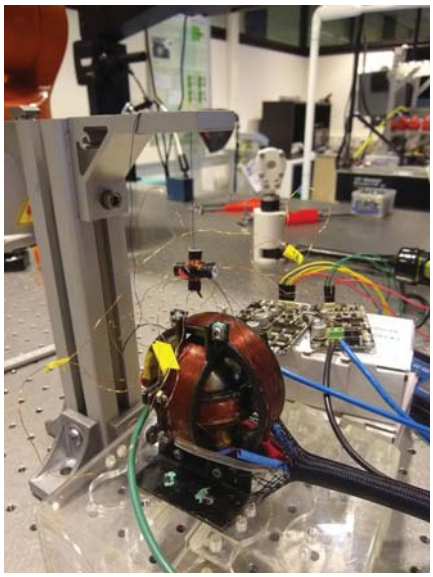

Fig. 8: Test setup in air with magnetic field generated by permanent magnet SEMA.

While performing these first test in air, the prototype did not show rotational movement. It was expected that the stiffness of the copper wires prevented the tri-axial coil from aligning with the magnetic field generated by the SEMA.
An estimation for the influence of the stiff copper wires on the prototype was done by calculating the stiffness torque, defined by:

$$\begin{aligned} \tau_k &= K_r\theta \\ &= \frac{\pi G d^4}{32L}\theta \end{aligned} \tag{21}$$

where G is the shear modulus of the wire material, d is the diameter of the wire, L is the length of the wire and θ is the angle. This equation is a measure for the torque that is needed to rotate the end of a wire. The values that were used to calculate the stiffness torque can be found in Table 1. The estimated

torque needed to overcome the stiffness in the wires was 687.0 mNm. In the physical experiments this value would be different, but this estimated torque is the order of magnitude we have to look at. This order of magnitude is much bigger than the theoretical magnetic torque, e.g. the stiffness could hinder the rotation of the prototype.

Table 1: Values used for calculating theoretical magnetic torque and stiffness torque.

Variable	**Value**	**Unit**
B	0.014	T
N	124	-
I	0.5	A
S	1.26e^{-5}	m^2
τ_m	12.3	mNm
G	44e^9	N/m^2
d	0.25	mm
L	0.05	m
θ	π/2	rad
τ_k	687.0	mNm

In conclusion, the prototype designed in this research did not show a change in orientation when the generated magnetic moment was exerted to a nonuniform magnetic field. This was presumable caused by thhe stiffness of the copper wires. Future prototype designs must take this stiffness into account, and contain a method of limiting or excluding this influence on the miniature robot.

Modelling the Magnetic Field of a Permanent Magnet Controlled by a 6-DOF Manipulator Using MATLAB

D. Jacob

University of Twente, Faculty of Engineering Technology – Drienerlolaan 5, 7522 NB, Enschede, The Netherlands
d.jacob@student.utwente.nl

ABSTRACT: To manipulate magnetic microrobots used for targeted drug delivery it is important to model the magnetic field that is created by a permanent magnet, which can be controlled three-dimensional space by a 6-DOF manipulator. Most studies implement specialist software to describe the behaviour of the manipulator. These however offer limited functionality, which makes it challenging to combine with a magnetic field simulation. This paper offers a complete simulation model from the manipulator kinematics to the magnetic field created by a rotating permanent grade52 NdFeB magnet. In this work the model KUKA KR10 R1100-2, which is a 6-axis robotic arm manipulator, is simulated in 3D space. The Denavit-Hartenberg representation is used to model the links and joints. The kinematic equations of motion and Jacobian matrix for the robot arm model are derived and implemented in MATLAB software. The simulations are visually supported by a graphical model of the KUKA robotic arm.

Key words: manipulator, robot modelling, forward and inverse kinematics, simulation, permanent magnet

1 INTRODUCTION

Helical microrobots are screw-shaped untethered devices, which are propelled by rotating magnetic fields. These microscopic devices hold great potential in the field of minimally invasive procedures for targeted therapy. Their movement resembles that of a cork- or woodscrew [1]. It is inspired by the locomotion observed with bacteria, which use their flagella as a helical propeller to be able to move in low-Reynolds flow [2]. Starting in 2007 first pioneering work was done on controlling artificial bacterial flagella with rotating magnetic fields [3], [4]. In the early works only closed configurations of electromagnetic coils are considered. A downside of such arrangements is their limited scalability, which makes them less suitable for *in vivo* applications. It was then proposed to use nonuniform magnetic fields generated by a single rotating magnet attached to a manipulator for steering [5]. Building on that Mahoney *et al.* addressed the issue of overcoming the attractive force and maximizing the torque, when using only a single rotating magnet [6], [7]. The rotating dipole field generates the torque on the microrobot, which induces the helical propulsion. The robotic manipulator enables the manipulation of the robot in a relatively large three-dimensional (3D) workspace.

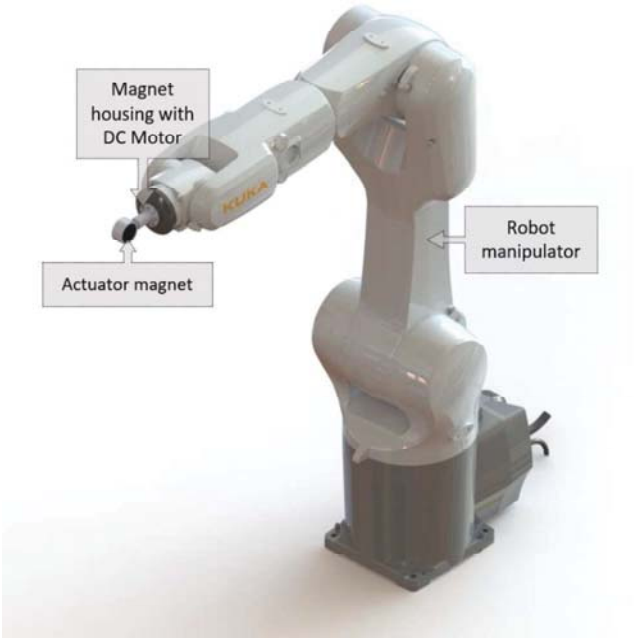

Fig. 1. A permanent magnet-based actuation system is simulated. The system consists of the 6-DOF KUKA robotic arm KR10-1100-2 and a cylindrical grade52 NdFeB magnet, which is attached to its end-effector. Between the end-effector and the magnet there is a DC motor, which causes the permanent magnet to rotate at a constant speed.

The purpose of this paper is to create a graphical simulation model in MATLAB for planning of future *in vitro* testing. The permanent magnet configuration implements the KUKA KR10 R1100-2 and a grade52